Evaluation of bending modulus of lipid bilayers using undulation and orientation analysis

Adarsh K. Chaurasia, Andrew M. Rukangu, Michael K. Philen, Gary D. Seidel, and Eric C. Freeman

Phys. Rev. E **97**, 032421 — Published 30 March 2018

DOI: 10.1103/PhysRevE.97.032421

Evaluation of Bending Modulus of Lipid Bilayers Using Undulation and Orientation Analysis

Adarsh K. Chaurasia, Andrew M. Rukangu, and Eric C. Freeman*

University of Georgia

Michael P. Philen and Gary D. Seidel

Virginia Tech

Abstract

In the current work, phospholipid bilayers are modeled using coarse grained molecular dynamics simulations with the MARTINI force field. The extracted molecular trajectories are analyzed using Fourier analysis of the undulations and orientation vectors to establish the differences between the two approaches for evaluating the bending modulus. The current work evaluates and extends the implementation of Fourier analysis for molecular trajectories using a weighted horizon based averaging approach. The effect of numerical parameters in the analysis of these trajectories is explored by conducting parametric studies. Computational modeling results are validated against experimentally characterized bending modulus of lipid membranes using shape fluctuation analysis. The computational framework is then used to estimate bending moduli for different types of lipids (PC, PE and PG). This work provides greater insight into the numerical aspects of evaluating bilayer bending modulus, provides validation for the orientation analysis technique and explores differences in bending moduli based on differences in lipid nanostructures.

Keywords: Lipid Bilayer, Bending Modulus, Coarse Grained, Molecular Dynamics, Fourier Analysis, Undulation Spectra, Orientation Spectra

* Corresponding Author, Assistant Professor, College of Engineering, University of Georgia, 101 Driftmier Engineering Centre, 597 D. W. Brooks Drive, Athens GA 30602, Ph:+1 (706)-542-4493 Email: ecfreema@uga.edu.

I. INTRODUCTION

Lipid bilayers form an important part of all living cells and help with regulation of cellular activity through the cell wall. These bilayers are primarily comprised of phospholipids which have a hydrophilic head and a hydrophobic tail, which in an aqueous environment results in self-assembly into bilayers with two layers of lipids across the membrane. It has been shown that in heterogeneous membranes made of several different lipid types, cell fusion processes are dependent on the reorganization (which can be related to the bending modulus) of these lipids into domains based on the local curvature to facilitate fusion [1–3]. In other words, lipids with small estimated bending modulus migrate to regions with larger curvature to reduce the total energy of fusion intermediates, highlighting the need to understand the bilayer bending modulus as a property of lipid nanostructure.

Computationally, the most commonly used method for evaluating the bending modulus for lipid bilayers is using molecular dynamics (MD) simulations to model 2D planar membranes and analyzing the thermal undulations from a flat planar initial structure through the power spectra of undulations [4–6]. The mathematical framework for this approach originated from the work of Helfrich [7] and Canham [8] which describes the free energy functional for thin membranes with no surface tension. A variational approach is then used to convert the curvature based energy functional to a function of deformation gradients. The energy functional is then converted to Fourier space assuming small deviations from the initial planar 2D structure. The power spectra of the undulations is observed to decay in the fourth power as a function of spatial frequency, with the associated constant dependent on the bilayer bending modulus. It is noted that the bilayer surface tension significantly affects the undulations of the membrane, and thus, affects the bending modulus obtained from the spectral analysis. Thus, the molecular simulations are performed at vanishing surface tension to reduce any significant influence on the estimated bending modulus.

A recent review [9] has shown that the undulation power spectra underpredicts the bilayer bending modulus as compared to experimentally reported values. An alternative approach based on the power spectra of lipid orientations in the membrane has been proposed in recent literature [10–12]. In this case, the energy functional for the bilayer includes the undulation, tilt and protrusion of lipids i.e. recognizing more local nanoscale (o(1nm)) deformations of the membrane as compared to the homogenized undulations (O(10nm)). In contrast to

the undulation based analysis which assumes that the lipid bilayer is a flat homogeneous continuum-like membrane, the orientation analysis recognizes the local molecular motion of the lipids in the bilayer and constructs an energy functional for each of these local modes of deformation. Orientation vectors are defined using the averaged heads and tails of these lipids as the unit vector connecting the heads to the tails. Time averaged power spectra of the orientation vector components is evaluated using 2D Fourier transforms and the bending modulus is estimated based on long wavelength convergence of the orientation power spectra. The orientation analysis is shown [9] to result in faster convergence i.e. a converged bending modulus is obtained from bilayers of a smaller size relative to the undulation analysis. The bending modulus obtained from the undulation spectra is expected to converge to those obtained from the orientation spectra as the size of the bilayer and the simulation times are increased. However, the time scale needed for the undulations to reach a converged estimate scales to the third power of the bilayer size [13]. These conditions result in simulating large bilayers over longer periods of time, which is computationally expensive. Thus, the orientation spectra based analysis has been preferred in recent publications [11, 12]. Some other computational methods reported in the literature for estimating the bilayer bending modulus include a) indirect estimation of bending modulus through area compressibility modulus [14] and b) bilayer buckling simulations [15].

While some studies published in the literature use full MD [6, 16], several computational studies in the literature use coarse grained (CG) MD simulations to study the undulations or orientation spectra [11, 12, 17]. Coarse grained molecular simulations significantly reduce the computation time by reducing the number of degrees of freedom in the system and by increasing the time step size. Of the several CG potentials developed in the past, MARTINI CG potentials [18, 19] were specifically designed and tested for modeling lipid based structures. The MARTINI potentials have been observed to reproduce structural observations like the area per lipid and lipid conformations, mechanical properties of the bilayers e.g. bending, tilt moduli, lipid aggregation and membrane domain formations [20]. Following from the literature, MARTINI force fields (martini22) will be used to perform the CG MD simulations of lipid bilayers in the current work.

Experimentally, a few different techniques have been used to determine the bending modulus of bilayers e.g. shape fluctuation (or flickering) analysis [21, 22], micropipette aspiration [23] and X-ray scattering [24]. A few reviews have outlined the various experimental meth-

ods and the estimates of bending moduli for a range of lipid types and influencing factors [25–28]. One of the issues with the bending modulus of lipid membranes is that the different experimental and computational techniques result in different values for the estimated modulus. A recent review [9] summarizes the current methods for finding the bilayer bending modulus from experiments and from computational molecular simulations, highlighting the differences in the results obtained from these techniques. It is concluded that the experimental and computational techniques used so far do not agree on the bending modulus, with up to 400% difference in bending moduli reported for bilayers composed of the same type of lipid. Thus, it is important to further verify the computational techniques used for estimating bilayer bending moduli and validate these with experimental results.

In this context, the current work is aimed at (a) evaluating the numerical implementation of the molecular trajectory analysis and extending the numerical techniques for more consistent estimation of bilayer properties, (b) verifying the estimated bending modulus with published literature and validating these with experimental characterization performed herein and (c) evaluating the bilayer bending modulus for more lipid types, i.e. phosphocholine (PC), phosphoethanolamine (PE) and phosphoglycerol (PG), using both undulation and orientation analysis to understand the effect of lipid nanostructure.

II. MATHEMATICAL PRELIMINARIES

The details of mathematical derivations for the undulation and orientation analysis can be found in [12]. However, a short description of key ideas is provided here. A schematic of a planar lipid bilayer undergoing thermal undulations is shown in Fig. 1. The undulation of the membrane is defined by the z coordinates of the mean lipid head surface. The surface obtained from lipid heads in the top leaflet is given by z^u(x,y) and the surface obtained from lipid heads in the bottom leaflet are given by z^l(x,y). The variation of the the central plane of the bilayer is then defined by $z = (z^u + z^l)/2$. The orientation vector for the membrane is defined as a unit vector $\mathbf{n}$(x,y) connecting averaged lipid heads to the averaged lipid tails in each leaflet. The orientation vector of lipids in the top leaflet is defined as $\mathbf{n^u}$(x,y) and the orientation of the lipids in the bottom leaflet is defined as $\mathbf{n^l}$(x,y). The unit vector normal to the homogenized surface of lipid heads is defined as $\mathbf{N^u}$(x,y) for the top leaflet and $\mathbf{N^l}$(x,y) for the bottom leaflet.

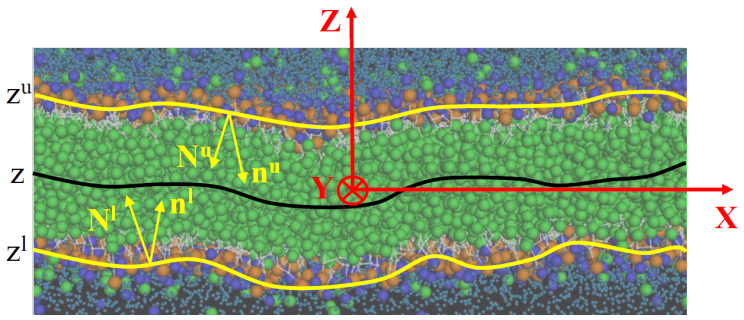

FIG. 1. Schematic of a lipid bilayer membrane with top and bottom leaflet undulation surfaces (z^u, z^l), mean bilayer undulation surface (z), the local unit normal perpendicular to the undulation surfaces ($\mathbf{N^u}$, $\mathbf{N^l}$) and local lipid orientation unit vectors ($\mathbf{n^u}$, $\mathbf{n^l}$).

The free energy of undulation for a bilayer using the Helfrich-Canham [7, 8] methodology for homogeneous thin membranes which lack internal structure (i.e. continuum based) is described as:

$$F_u = \frac{1}{2}\int\int \left(k_c|\nabla^2 z|^2+\gamma|\nabla z|^2\right) dA \tag{1}$$

where k_c is the bending modulus of the membrane and γ is the surface tension. The expression for free energy presented in Eqn. 1 further assumes that the membrane is symmetric (i.e. has same lipid composition and density in each leaflet) and the leaflets are exposed to the same aqueous environment on either sides of the bilayer, such that there is negligible spontaneous curvature. This equation is converted to Fourier space by performing a Fourier transformation, i.e. $z(\mathbf{x}) = \sum_q \hat{z}(\mathbf{q})e^{i\mathbf{q}\cdot\mathbf{x}}$. The Fourier transformation converts the undulation variable z from 2D Cartesian space $\mathbf{x} = (x, y)$ to 2D Fourier space $\mathbf{q} = (q_x, q_y)$. The quadratic form of the free energy allows for using the equipartition theorem which states that the energy stored in each of the modes is equal to $\frac{1}{2}k_BT$ and results in the following relationship:

$$\left\langle|\hat{z}(\mathbf{q})|^2\right\rangle = \frac{k_BT}{k_c|q|^4+\gamma|q|^2} \tag{2}$$

where $\langle|\hat{z}(\mathbf{q})|^2\rangle$ is time averaged magnitude of the power spectra of undulations, k_B is Boltzmann's constant and T is the temperature. For large values of q, or if there is significant surface tension in the membrane, the second term in the denominator governs the power

spectra of undulations. However, for small values of q and tensionless membranes, the first term in the denominator governs the power spectra. Under the assumption of vanishing bilayer surface tension and small q (i.e. long spatial wavelength), the power spectra can be approximated as:

$$\left\langle |\hat{z}(\mathbf{q})|^2 \right\rangle = \frac{k_B T}{k_c |q|^4} \tag{3}$$

If the local lipid structure of the membrane is considered, and an assumption of small undulations is placed, the bilayer free energy for undulation can be described in terms of the local lipid orientation vectors [11] as:

$$F_u = \frac{1}{2} \int \int \left(k_c (\nabla \cdot \mathbf{n})^2 - \frac{\Omega}{b_0} \varepsilon \nabla \cdot \mathbf{n} + \frac{K_A}{b_0^2} \varepsilon^2 + K_\theta \mathbf{m}^2 + K_{tw} (\nabla \times \mathbf{m})^2 \right) dA \tag{4}$$

where Ω is the bending-compression coupling coefficient, K_A is the area compressibility modulus, K_θ is the tilt modulus, K_{tw} is the twist modulus, $\varepsilon = \tilde{z} - z$ where $\tilde{z}$ is the homogenized mid surface, b_0 is the mean bilayer thickness and $\mathbf{m} = \mathbf{n} - \nabla z$ assuming small undulations. Similar to undulation analysis, Fourier transformation converts the orientation vector components from Cartesian to Fourier space as $\mathbf{n}(\mathbf{x}) = \sum_q \hat{\mathbf{n}}(\mathbf{q}) e^{i\mathbf{q}\cdot\mathbf{x}}$. Furthermore, a new definition for longitudinal orientation vector in the Fourier space may used as $\hat{\mathbf{n}}^{||}(\mathbf{q}) = \frac{1}{|q|}[\mathbf{q} \cdot \hat{\mathbf{n}}(\mathbf{q})]$, where $|q|$ is the element-wise norm of the wavevector defined as $|q| = \sqrt{q_x^2 + q_y^2}$. After using the equipartition theorem, the time averaged magnitude of the power spectra for longitudinal orientation vector ($\left\langle |\hat{\mathbf{n}}^{||}(\mathbf{q})|^2 \right\rangle$) is decoupled and is given by:

$$\left\langle |\hat{\mathbf{n}}^{||}(\mathbf{q})|^2 \right\rangle = \frac{k_B T}{k_c |q|^2} \tag{5}$$

Unlike the undulation spectra (Eqn. 3) which decays as the fourth power of q, the orientation spectra decays as the second power of q for long spatial wavelengths.

III. MODELING AND ANALYSIS

Computational modeling of lipid bilayers is performed using CG MD in Gromacs 5.1 and the 2D Fourier analysis is performed using in-house Python 2.0 scripts parallelized by Python's multiprocessing module. Details of the numerical aspects of modeling and analysis are provided here.

III.1. Coarse Grained Molecular Dynamics

The coarse grained molecular modeling of the bilayers is performed using the MARTINI CG force field in Gromacs. The bilayers are assembled using a script [29] to set up a simulation box with a flat lipid bilayer, water molecules and salt ions (Na^+, Cl^-). It is to be noted that the number of lipids in each leaflet is the same in the initial assembly and the aqueous environment on either sides of the bilayer is the same, such that there is negligible spontaneous curvature in the membrane. The system is minimized using the steepest decent algorithm for 10000 steps. Once the structure is minimized, the production runs are performed using an NPT ensemble for 400ns with a time step of 40ps. The reference temperature is fixed at 325K and a surface-tension pressure coupling is used with zero in-plane surface tension and 1 atm pressure along the bilayer thickness direction. The surface-tension pressure coupling in Gromacs allows for the MD box size (or bilayer in-plane dimensions) to evolve to statistically maintain a prescribed surface tension (zero for the current work). Periodic boundary conditions are used in all three spatial directions.

Molecular trajectories for the lipid heads and the lipid tails are extracted every 0.4ns for analysis after the first 80ns equilibriation time such that the analysis results shows small variations. The molecular trajectories are extracted for the heads and tails for both the upper and lower leaflets. The lipid heads are defined by averaging the coordinates of the two linker glycerol groups and the tails are defined by averaging the coordinates of the end acyl groups in lipid tails. It has been shown [16] that different choices of lipid head and tail estimation results in small variations in the evaluation of bending modulus. For the analysis, the trajectories are divided into time blocks of 40ns which each block analyzed individually to establish error estimates in estimated bending modulus, similar to the block averaging process used in [16].

III.2. Fourier Analysis

The trajectories of the lipid head and tail groups are sorted into the upper leaflet and lower leaflet based on the averaged lipid head coordinates. These trajectories are subsequently used to evaluate averaged undulation coordinates (z) and orientation vector components (n_x,n_y) as:

$$z = \frac{z^u + z^l}{2} \tag{6a}$$

$$n_x = \frac{n_x^u - n_x^l}{2} \tag{6b}$$

$$n_y = \frac{n_y^u - n_y^l}{2} \tag{6c}$$

One of the keys to finding the 2D Fourier transform for the undulation variable (z) or the orientation vector components (n_x,n_y) is interpolating the unstructured molecular head/tail particle data to a structured grid. Some studies in the literature [11, 12] have averaged the data in each cell of structured grid to estimate the averaged quantities for each of the grid points. However, this method leads to issues with empty grid cells as the number of grid points is increased (which is important for better resolution and accuracy of the obtained Fourier transform). Consequently, larger grid cells (or smaller number of structured grid points) are used for Fourier analysis i.e. a larger section of the 2D data is averaged. It has been pointed out [30] that averaging over larger sections may lead to reduction the Fourier spectra magnitude, especially for fast varying spatial data (e.g. local orientation vector components in the current work). In order to lift these constraints, a non local weighted averaging method (similar in principle to [29]) is used in the current work. Undulation coordinates and orientation vector components are averaged over a radius of size δ on a structured grid as shown in the schematic in Fig. 2a,2b. The radius (δ) over which the undulation and orientation variables are averaged is called the horizon.

It is to be noted that the horizon radius follows the rules of periodic boundary conditions in both x and y directions as indicated in Fig. 2b. Averaging over a horizon interpolates the unstructured data onto a defined regular N $\times$ N square grid, with grid points defined as $\tilde{\mathbf{x}}_i$. In general, a field variable given by $f(\mathbf{x})$ is averaged as:

$$f(\tilde{\mathbf{x}}_i) = \frac{1}{\int_{A_c} w(r_{\mathbf{x}}) dA} \left[\int_{A_c} w(r_{\mathbf{x}}) f(\mathbf{x}) dA \right] = \frac{1}{\sum_{j=1}^{N_c} w(r_{\mathbf{x}_j})} \left[\sum_{j=1}^{N_c} w(r_{\mathbf{x}_j}) f(\mathbf{x}_j) \right] \tag{7}$$

where A_c is defined as the area of a circle centered at $\tilde{\mathbf{x}}_i$ and a radius of δ, $w(r_{\mathbf{x}_j})$ is the weight assigned to a particle at a radius $r_{\mathbf{x}_j}$ away from $\tilde{\mathbf{x}}_i$ and N_c is the number of particles which lie inside the horizon. For the current work, the field variables defined by $f(\mathbf{x})$ are the undulation variable (z) and the components of the orientation vector (n_x, n_y). The weights assigned to the particles, $w(r_{\mathbf{x}_j})$ are defined as:

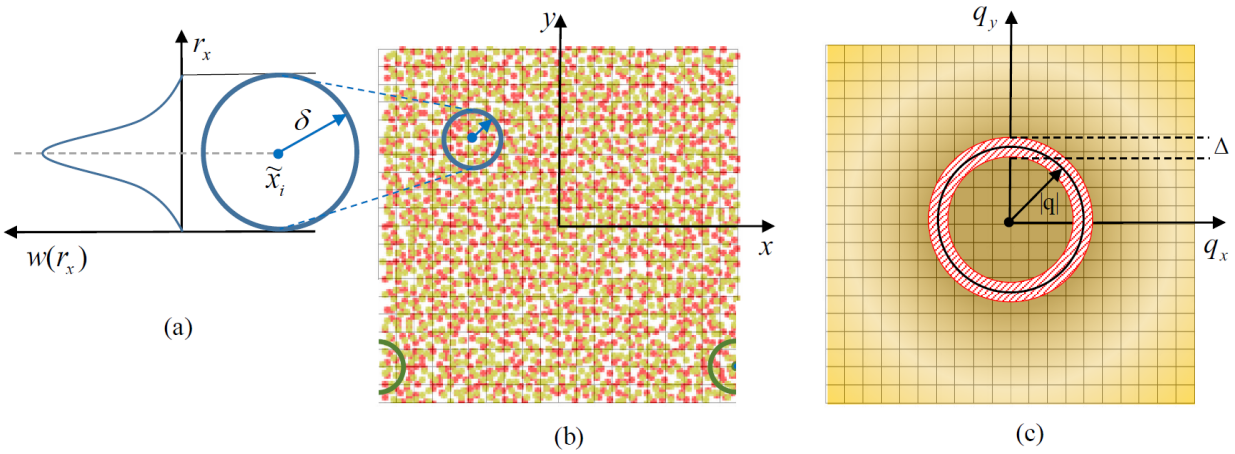

FIG. 2. Schematic of a) the weighted horizon over one structured grid point ($\tilde{\mathbf{x}}_i$), b) local horizons overlaid on the structured mesh and unstructured molecular data indicating periodicity of horizons and c) radial binning averaging over annular patches using a binwidth Δ to convert from 2D to 1D Fourier space.

$$w(r_{\mathbf{x}_j}) = \frac{1}{1 - \mathrm{e}^{-\alpha}} \left[\mathrm{e}^{-\alpha r_{\mathbf{x}_j}/\delta} - \mathrm{e}^{-\alpha} \right] \tag{8}$$

where the weight decreases exponentially away from the center, $\tilde{\mathbf{x}}_i$, at a rate defined by the exponent α and becomes zero at $r_{\mathbf{x}_j} = \delta$. The horizon based averaging scheme used in the current work circumvents issues with the grid based approach [11, 12], i.e. cells with no lipids, for a fine structured grid. The combination of the horizon radius and exponent α in the weighing function may be adjusted to allow for a finer structured grid preserving the local perturbations in the undulation and orientation variables. The fast decaying exponential weighing function rapidly reduces the influence of lipids further away from the center rapidly, preserving the local perturbations in data extracted from molecular trajectories. Fig. 3a shows the molecular trajectories for a lipid bilayer of size ∼32nm square undergoing undulations. Fig. 3b and Fig. 3c show the averaged undulation ($\tilde{z}$) and orientation component ($\tilde{n}_x$) using a horizon radius of 2nm with α=8 and N=32. The particles in the foreground are the positions of averaged lipid heads which are colored based on the local values of z and n_x. The background shows the contour of the field variables after they are interpolated to a regular background mesh using weighed averaging i.e. $\tilde{z}$ and $\tilde{n}_x$. It is to be noted that the $\tilde{z}$ shows a long range variation whereas $\tilde{n}_x$ shows local perturbations in the orientation vector components. The local variations in the orientation vector components

results in faster convergence to the bending modulus relative to the undulation analysis since the time scales associated with the changes in lipid orientations are smaller.

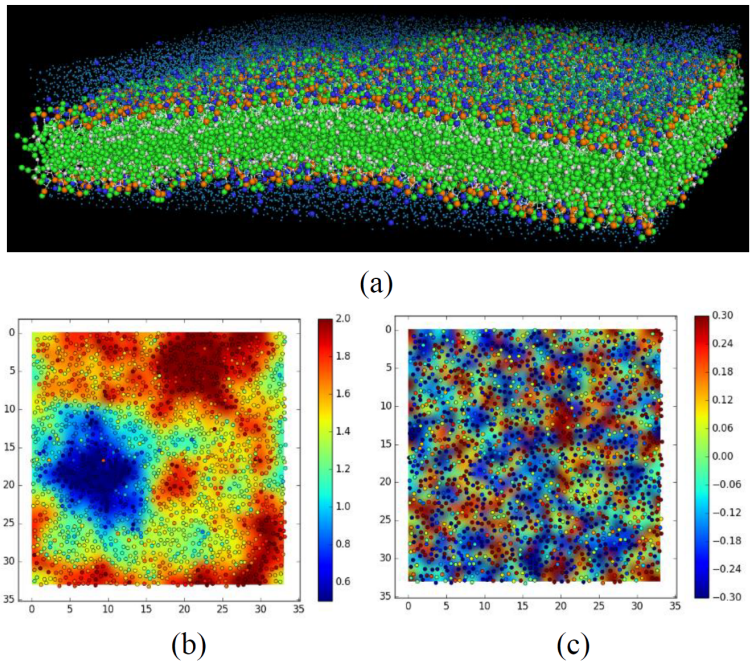

FIG. 3. a) Coarse grained representation of a lipid bilayer (∼32nm) membrane modeled using MARTINI potentials in Gromacs, b) 2D contours of local lipid undulation overlaid on averaged undulation field variable using a horizon radius (δ) of 2nm with α=8 and N=32 c) 2D contours of local lipid orientation overlaid on averaged orientation field variable using a horizon radius (δ) of 2nm with α=8 and N=32.

After the interpolation to a structured grid is performed, 2D Fourier analysis can be performed using standard discrete Fourier transform tools. At this point the variables of interest $(\tilde{z}, \tilde{n}_x, \tilde{n}_y)$ convert from the real space $(\mathbf{x})$ to Fourier space $(\mathbf{q})$ and are denoted by $(\hat{z}, \hat{n}_x, \hat{n}_y)$ where $(\hat{\cdot})$ denotes that the variables are now defined on Fourier space $\mathbf{q} = (q_x, q_y)$. The orientation vector components in the Fourier space are further used to evaluate the longitudinal orientation vector as:

$$\hat{\mathbf{n}}^{||} = \frac{1}{|q|}\left[\mathbf{q} \cdot \hat{\mathbf{n}}\right] = \frac{1}{|q|}\left[q_x \hat{n}_x + q_y \hat{n}_y\right] \tag{9}$$

where $|q|$ is the element-wise norm of the wavevector defined as $|q| = \sqrt{q_x^2 + q_y^2}$. The field variables of interest $(\hat{z}, \hat{n}^{||})$ are converted from 2D to 1D Fourier space by recognizing the radial symmetry in 2D Fourier space and performing radial averaging using wavevector

binning (Fig. 2c). Let us say a field variable, $\hat{f}(q_x, q_y)$ is defined on a 2D Fourier space. The variable can be represented on a 1D Fourier space using wavevector binning as:

$$\hat{f}(|q|) = \int_{|q|-\Delta/2}^{|q|+\Delta/2} \left\langle \hat{f}(q_x, q_y) \right\rangle \, d|q| = \frac{1}{N_q} \sum_{N_q} \hat{f}(q_x, q_y) \tag{10}$$

where $\langle \cdot \rangle$ denotes averaging over the binwidth $\Delta = \pi/L$ in the current work and N_q are the number of points in the bin.

IV. EXPERIMENTAL CHARACTERIZATION

IV.1. Vesicle Generation

Giant unilamellar vesicles (GUVs) are formed using the electroformation technique [31–33] and used to study bilayer bending modulus experimentally. A polydimethysiloxane (PDMS, Sylgard 184, Dow Corning) mold is created with a hydrating well of cylindrical cross section as shown in Fig. 4. The mold is sandwiched between two conductive surfaces which act as electrodes. For the current work, 10mg of 1,2-diphytanoyl-sn-glycero-3-phosphocholine (DPhPC, Avanti Polar Lipids) lipids are dissolved in 1mL of chloroform and transferred to a 10ml scintillating vial. A solution with 5μL of the lipids in chloroform are deposited onto the conducting surface of the bottom indium tin oxide (ITO, Sigma Aldrich) slide using a glass pipette. Nitrogen or Argon (Airgas) gas is passed over the lipids for three minutes to coat an even thin film over the ITO slide. The coated ITO slide is placed under vacuum for 1 hour to evaporate remaining excess chloroform from the lipids. The top ITO slide is placed onto the PDMS substrate and bottom ITO slide encapsulating the hydrating well. A hydrating solution is introduced into the well allowing for swelling of lipid layers into GUVs. A syringe with a 1mm blunt needle attachment is used to inject the hydrating solution, 20mM sucrose (Sigma Aldrich) in deionized (DI) water, through specially included channels in the sides of the PDMS mold. Finally, a sinusoidal AC waveform is applied across the chamber to trigger the budding and swelling of vesicles. In the current work, an AC waveform of amplitude of 1V and a frequency of 1Hz was passed through the ITO slides for 3 hours. Varying the electric potential and frequency produces GUVs of different sizes. At this point, the well contains electroformed GUVs which are extracted by a syringe pump to prevent vesicle collapse, and transferred to dishes for observation. Other techniques for

generation of GUVs include phase transfer [21] and sonication/extrusion [34].

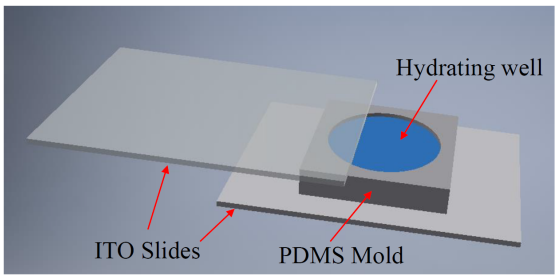

FIG. 4. Illustration of the electroformation setup for vesicle generation.

IV.2. Experimental Evaluation of Bending Modulus

The images of GUVs in solution are captured by an inverted brightfield microscope. A band pass filter is used on the images to enhance the GUV outlines. A gradient based approach is used to extract the contours of liposomes where a combination of first and second derivatives of the pixel intensity are used to define the contours.

A detailed description of image analysis for the GUVs to estimate the bending modulus may be found in [17, 35] and references therein. However, the key ideas are outlined here. For the experimentally observed GUVs, the X-Z plane of the bilayer (Fig. 1) is observed as a circular outline of the vesicles. The undulations of the circular vesicle are observed as the variations in radial displacement. In this case, the equations presented in Section II for flat planar bilayers need to be extended by using an equatorial projection [17, 35] and can be represented as:

$$\left\langle |\hat{u}(\mathbf{q})|^2 \right\rangle = \frac{k_B T}{2L\gamma} \left[\frac{1}{q} - \frac{1}{\sqrt{\frac{\gamma}{k_c} + q^2}} \right] \tag{11}$$

where $\langle |\hat{u}(\mathbf{q})|^2 \rangle$ is the time averaged magnitude of the power spectra for the radial displacements. Under the assumption of long wavelengths and small surface tension, Eqn. 11 reduces to:

$$\left\langle |\hat{u}(\mathbf{q})|^2 \right\rangle = \frac{k_B T}{4L k_c |q|^3} \tag{12}$$

where $L = 2\pi \langle r \rangle$ is the averaged circumference of the vesicle with $\langle r \rangle$ being the average radius. The power spectra of experimentally observed radial undulations of the GUVs from an initial spherical shape decays as a third power of q as against the fourth power for planar bilayer using the undulation analysis (Eqn. 3).

V. RESULTS AND DISCUSSION

V.1. Experimental Results

Experimental investigation is performed with 1,2-diphytanoyl-sn-glycero-3-phosphocholine (DPhPC) liposomes to validate the bending modulus estimates obtained from the computational framework. DPhPC lipids are chosen in the current work since the liposomes are stable for a large range of temperature and physiological conditions. The coarse grained representation of DPhPC lipids using MARTINI CG is the same as DPPC, since MARINI CG represents butane and isopropane using the same effective atom [18, 19]. Thus, the computational results for DPPC bilayers are directly comparable with the experimental investigation with DPhPC liposomes. Fig. 5 shows a GUV with $\sim$70μm diameter as observed from the microscope (Fig. 5a) and with the extracted contour using subsequent image analysis (Fig. 5b). The extracted contour is further used to perform Fourier analysis as discussed in Section IV.2 and averaged over $\sim$1150 time frames. The resulting power spectra of the radial undulation ($\hat{u}_q$) normalized by q^3 is shown in Fig. 5c. It is to be noted that the converged value of $q^3 \langle |\hat{u}_q|^2 \rangle$ for small q is used to estimate the bending modulus of the bilayer using Eqn. 12. For the three liposomes the study was performed, the estimated bending moduli were observed to be $12.84 \pm 1.97 \times 10^{-20}$J.

V.2. Effect of Interpolation Parameters

One of the keys to estimating the bending modulus is understanding the influence of trajectory analysis parameters on the averaging of molecular trajectories and the subsequent Fourier analysis. This is specially important, since the estimated bending modulus may vary significantly depending on the choice of these parameters. In the studies presented in the literature [10–12, 15], the emphasis is on highlighting the mathematical framework and demonstrating its applicability in comparison to previously published experimental results.

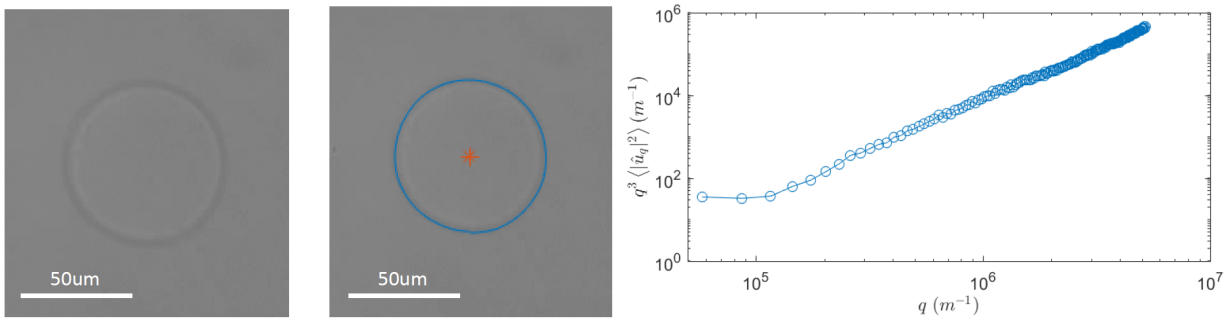

(a) (b) (c)

FIG. 5. a) Sample of one time frame of a GUV (∼70μm diameter) observed under the microscope, b) extracted GUV contour using image analysis and c) normalized power spectra for radial undulations ($q^3\left\langle|\hat{u}_q|^2\right\rangle$) for a DPhPC liposome.

However, the role of interpolation parameters has not been sufficiently addressed. In the current work, parametric studies are conducted by varying three key analysis parameters which affect the estimated bending modulus, i.e. horizon radius (δ), weighing function exponent (α) and the number of regular grid points (N), to understand their influence on the estimated bending moduli, following from Eqns. 7 and 8.

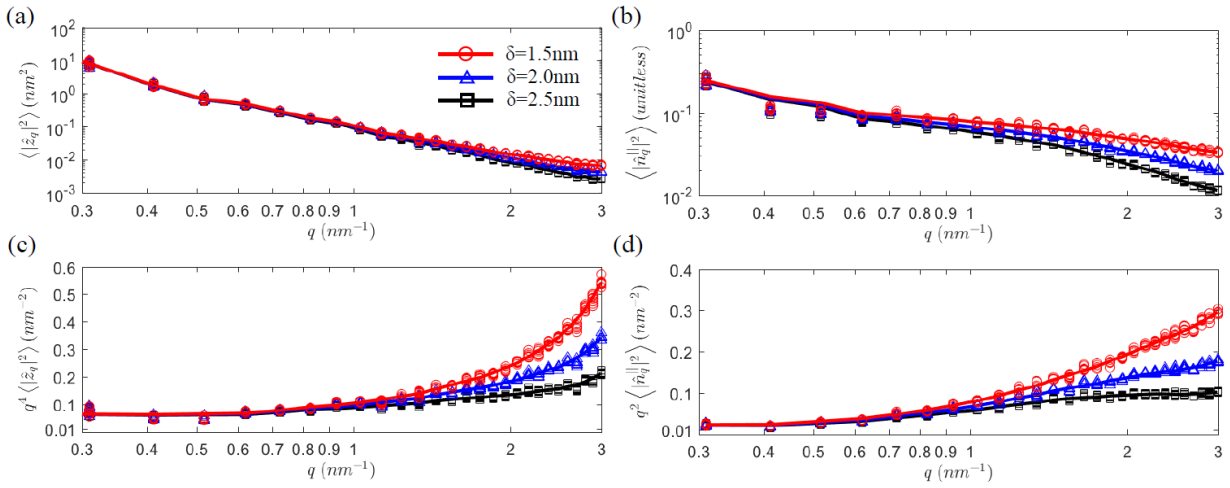

FIG. 6. Time averaged a) undulation spectra, b) orientation spectra, c) normalized undulation spectra and d) normalized orientation spectra for a ∼32nm DPPC bilayer with α=8 and N=32 for different horizon radii (δ).

A comparison of power spectra obtained from the undulation and orientation analysis for a 1,2-dipalmitoyl-sn-glycero-3-phosphocholine (DPPC) bilayer (∼32nm) for different horizon

radii are shown in Fig. 6. Fig. 6a shows the power spectra obtained from the undulation analysis ($\langle|\hat{z}_q|^2\rangle$), Fig. 6b shows the power spectra obtained from the orientation analysis ($\left\langle|\hat{n}_q^{||}|^2\right\rangle$), Fig. 6c shows the normalized power spectra from undulation analysis ($q^4\,\langle|\hat{z}_q|^2\rangle$) and Fig. 6d shows the normalized power spectra from orientation analysis ($q^2\left\langle|\hat{n}_q^{||}|^2\right\rangle$). The data points represent the magnitude of power spectra obtained from each of the 40ns time blocks and the solid line represents the best fit to the block averaged data points. For the results presented in Fig. 6, the weight function exponent (α) is chosen to be 8 and the grid size (N) is 32 i.e. the horizon spans nearly two regular grid cells for 2nm horizon size. It is to be noted that the converged small q magnitudes for the normalized undulation and orientation spectra are used to estimate the bending moduli using Eqns. 3 and 5. It is observed that a larger horizon radius results in a decrease in the magnitude for short wavelength (large q) undulation and orientations spectra. Averaging over a larger radius cancels out the local perturbations in the trajectories around a mean value and results in a decreased magnitude. This is especially true for the orientation components since they exhibit local fast varying perturbations. Thus, the reduction in the magnitude for large q is more significant in the orientation spectra as compared to the undulation spectra.

TABLE I. Estimated bending moduli for a DPPC bilayer from undulation and orientation analysis for different horizon radii (δ) with α=8 and N=32.

Horizon Radius δ (nm)	Undulation Analysis k_c ($\times 10^{-20}$J)	Orientation Analysis k_c ($\times 10^{-20}$J)
1.5	6.90	15.24
2	6.99	16.34
2.5	7.11	17.27

While the normalized power spectra from the undulation and orientation analysis seem to converge for long wavelengths (small q) from Fig. 6, small variations in the converged magnitudes may result in considerable differences in estimated bending moduli. The bending moduli for the three horizon radii studied here (1.5nm, 2nm and 2.5nm) with α=8 and N=32 are presented in Tab. I. It is to be noted that a horizon radius of 1.5nm is the smallest permissible in this case since a smaller horizon size leads to no enclosed lipids in the horizon at some of the analysis time steps. The smallest permissible horizon radius

will, in general, be dependent on the area per lipid of the bilayer such that each horizon over each grid point is occupied by at least one lipid for the entire length of time of the simulations. It is observed that a larger horizon radius results in a larger estimate for the bending modulus since a larger horizon leads to smaller magnitude of the converged time averaged spectra. While the difference in the converged magnitude is small, it still leads to a small increase in bending moduli with increasing horizon radius as the bending moduli are inversely related to the normalized magnitude of the power spectra for small q in Eqns. 3 and 5. The increase in bending moduli estimated from undulation analysis and the orientation analysis are observed to be $\sim$3% and $\sim$13%, respectively, between cases with δ=1.5nm and δ=2.5nm. The larger difference observed for the orientation analysis is because the local perturbations in orientation vector components get averaged out for a larger horizon radius. In addition, Tab. I shows that the estimated bending moduli from the undulation analysis are significantly smaller than those obtained from the orientation analysis similar to the observations reported in the literature [9]. The undulations are expected take a larger bilayer size and a longer simulation time to converge to the results obtained from the orientation analysis.

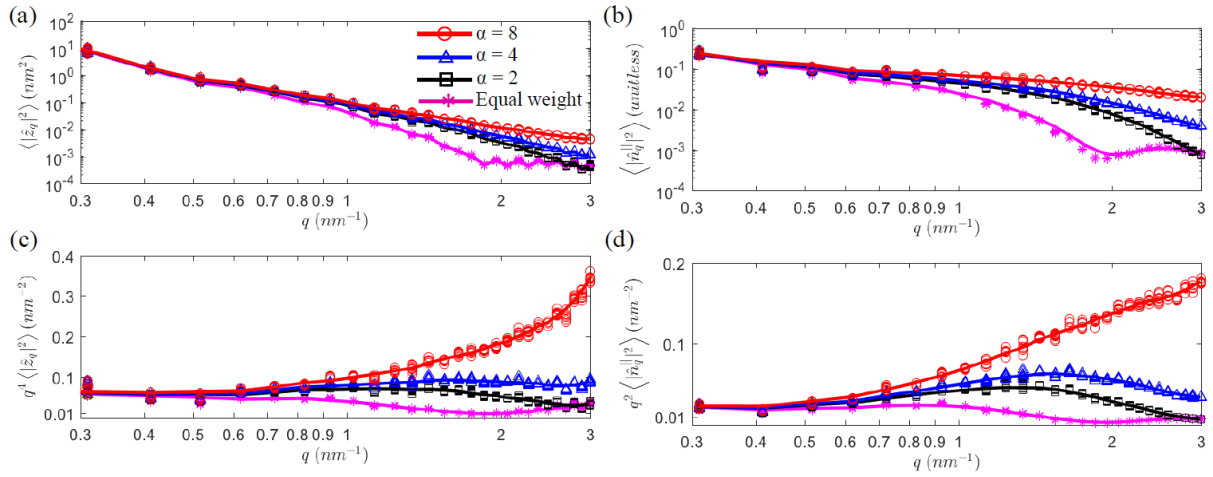

FIG. 7. Time averaged a) undulation spectra, b) orientation spectra, c) normalized undulation spectra and d) normalized orientation spectra for a $\sim$32nm DPPC bilayer with δ=2nm and N=32 for different weight function exponents (α) and a case with equal weights.

The power spectra obtained from the undulation and orientation analysis for different exponents (α) of the weighing function are shown in Fig. 7 in comparison to a case with

equal weighing of all particles within the horizon (as used in [11, 12]). The weighing function introduced in Eqn. 8 is defined as $w(r_{\mathbf{x}_j}) = 1$ for the case with equal weights. For the results presented in Fig. 7, a horizon radius of 2nm is chosen and the grid size is 32. It is observed that the magnitude of the power spectra decreases as α is decreased from 8 to 2, especially for large q. A larger weighing function exponent allows for capturing local perturbations in the undulation and orientation analysis as compared to smaller exponents. Thus, the magnitude gets smaller as the local perturbations get averaged for smaller exponents. The case of equal weights (as used in [11, 12]) shows significantly smaller magnitude even for moderately small values of q. Tab. II presents the estimated bending moduli from each of the cases shown in Fig. 7. The estimated bending moduli gets larger as the weight function exponent is reduced from 8 to 2 and finally to a case with equal weights. These estimated follow from the smaller magnitude of power spectra for small exponents and equal weight case. Similar to the horizon radius comparison, the observed change in bending moduli are larger for orientation analysis as compared to the undulation analysis. For example, the difference between cases with α=8 and α=2 is $\sim$5% from the undulation analysis and $\sim$14% from the orientation analysis. The estimates of bending moduli case with equal weights is remarkably larger as compared to any of the cases with weighted horizon averaging.

TABLE II. Estimated bending moduli for a DPPC bilayer from undulation and orientation analysis for different weight function exponents (α) and a case with equal weights using δ=2nm and N=32.

Weight Function Exponent α	Undulation Analysis k_c ($\times 10^{-20}$J)	Orientation Analysis k_c ($\times 10^{-20}$J)
8	6.99	16.34
4	7.22	18.19
2	7.37	19.06
Equal Weights	7.98	22.20

The power spectra obtained for different grid size (N) from the undulation and orientation analysis are shown in Fig. 8. For these results, the horizon radius and the weight function exponent are chosen to be 2nm and 8, respectively. The case with N=18 (as used in [11, 12], but with grid based averaging) is significantly under-sampled and leads to a larger power spectra magnitude, especially for the orientation analysis where the magnitude is

significantly large for all values of q. The magnitude is further observed to decrease slightly with increasing number of grid points, especially for large q. However, as seen earlier, small variations in low q magnitude may lead to significant variations in the estimated bending moduli. Tab. III shows a comparison of the estimated bending moduli for each of the cases presented in Fig. 8. The case with N=18 shows significantly smaller estimated bending modulus based on the large magnitude of the power spectra, especially from the orientation analysis where the under-sampling is more prominent because of the local variations in orientation vector components. As N increases further, the estimated bending modulus increases at a successively smaller rate showing convergence in the estimated modulus.

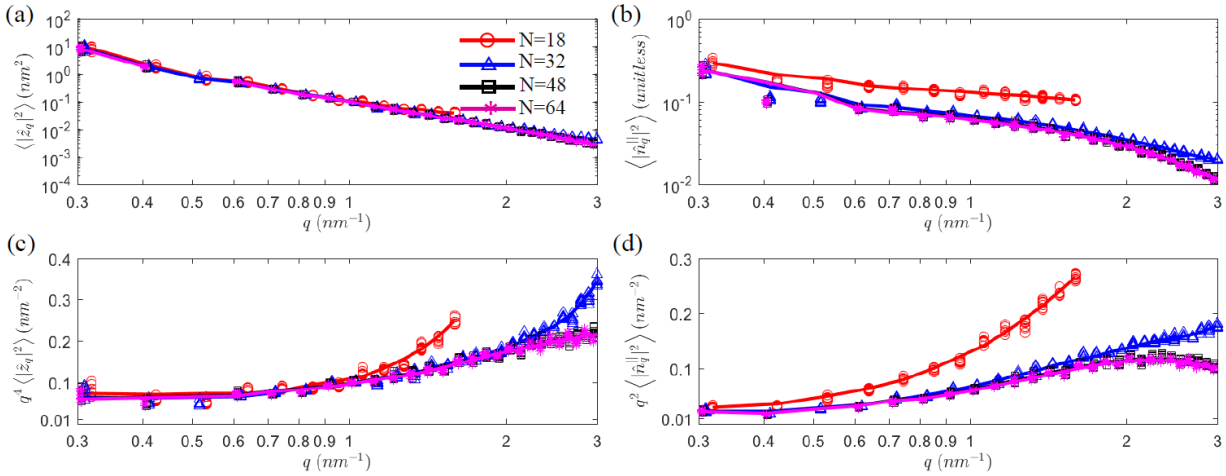

FIG. 8. Time averaged a) undulation spectra, b) orientation spectra, c) normalized undulation spectra and d) normalized orientation spectra for a ∼32nm DPPC bilayer with δ=2nm and α=8 for different grid sizes (N).

TABLE III. Estimated bending moduli for a DPPC bilayer from undulation and orientation analysis for different grid sizes (N) with δ=2nm and α=8.

Grid Size N	Undulation Analysis k_c ($\times 10^{-20}$J)	Orientation Analysis k_c ($\times 10^{-20}$J)
18	6.13	9.96
32	6.99	16.34
48	7.03	17.43
64	7.20	17.82

The results presented here show that the choice of interpolation parameters may lead to differences in the power spectra magnitude, and thus, in estimation of bilayer bending moduli. This difference is larger for the bending moduli estimated using the orientation analysis, since the local perturbations in orientation vector components makes it more sensitive to these parameters. In choosing these parameters, the key is to preserve the local values as far a possible during the averaging i.e. using small horizon radius and large α. In addition, the number of regular grid points (N) should be sufficiently large to sample the space sufficiently. However, any averaging or interpolation scheme (from unstructured to structured data) would lead to slightly smaller power spectra magnitude, and thus, a slightly larger estimated bending modulus.

TABLE IV. Bending moduli reported in the literature for DPPC bilayers from computational and experimental studies in comparison to those estimated in the current work. (Note: DPPC and DPhPC have the same MARTINI CG structure)

Reference	Type of Study	Size (number of lipids), time (μs)	k_c ($\times 10^{-20}$J)
Previously Published Literature			
DPPC [18]	Undulation Analysis (CG)	6400, 0.15	4.0
DPPC [4]	Undulation Analysis (Full Atomistic)	1024, 0.01	5.7
DPPC [6]	Undulation with tilt correction (CG)	3200, 1	21.0
DPPC [11]	Orientation Analysis (MARTINI)	2048, 2.4	13.0
DPPC [11]	Orientation Analysis (Unified Atom CG)	2048, 2.4	16.0
DPPC [16]	Orientation Analysis (CHARMM)	648, 0.11	15.6
DPPC [9]	Buckling Analysis (MARTINI)	640, 4	14.6
DPPC [36]	Shape Fluctuation Analysis (Experimental)	-	15.0
Current Work			
DPPC	Undulation Analysis (MARTINI)	3200, 0.4	6.99
DPPC	Orientation Analysis (MARTINI)	3200, 0.4	16.34
DPhPC	Shape Fluctuation Analysis (Experimental)	-	12.84 $\pm$ 1.97

For further verification, the results obtained from undulation and orientation analysis are compared with the literature. Table IV shows the bending modulus for DPPC bilayers

reported in the literature and those estimated in the current work. The bending moduli reported in the literature from the undulation analysis are much smaller in comparison to those with the tilt correction (which requires prior knowledge of the tilt modulus - see Table IV ref [6]) or the orientation analysis. In addition, the orientation analysis results reported in the literature are observed to predict the experimentally observed estimates more closely in comparison to other computational modeling methods [9]. The estimated bending modulus obtained in the current work using the undulation analysis is significantly smaller from the experimental results obtained herein (Sec. V.1), as has been the case with earlier literature. However, the estimated bending moduli from the undulation analysis obtained in the current work are close to similar computational studies performed previously. The bending modulus obtained from the orientation spectra based analysis in the current work is observed to be close to the experimental results, both in the current work and those published earlier.

V.3. Bending modulus of different lipid membranes

After the computational framework is verified and validated, it is further used to estimate the bending moduli for bilayers with different lipid types. In addition to the DPPC bilayer studied herein, 1,2-dioleoyl-sn-glycero-3-phosphocholine (DOPC), 1,2-dioleoyl- sn-glycero-3-phosphoethanolamine (DOPE) and 1,2-dioleoyl-sn-glycero-3-phospho-(1'-rac-glycerol) (DOPG) bilayers are studied to understand the effect of differences in head and tail groups on the estimated bending moduli. The lipids DOPC, DOPE and DOPG have the same tail group and are of the same size, but have different head groups as shown in Fig. 9. Fig. 10a-10c shows the undulation spectra for the three lipid types and Fig. 10d-10e show the normalized undulation spectra. Corresponding estimates of bending moduli for these bilayers are presented in Tab. V along with the computational and experimental results available in the literature. Following from the observations made earlier, the bending moduli estimates obtained from the undulation analysis underpredict the experimentally observed bilayer bending modulus.

Fig. 11a-11c shows the orientation spectra for the three lipid types and Fig. 11d-11e show the normalized orientation spectra. Corresponding estimates of bending moduli for these bilayers are presented in Tab. V. The estimates from orientation analysis are close to those

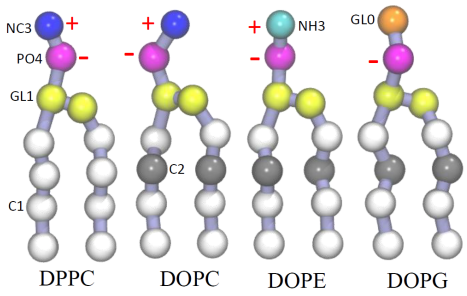

FIG. 9. Coarse grained lipid nanostructure for DPPC, DOPC, DOPE and DOPG lipids (NC3: choline, PO4: Phosphate, C1: butane/isopropane, C2: butene, NH3: Amine, GL0: Glycerol).

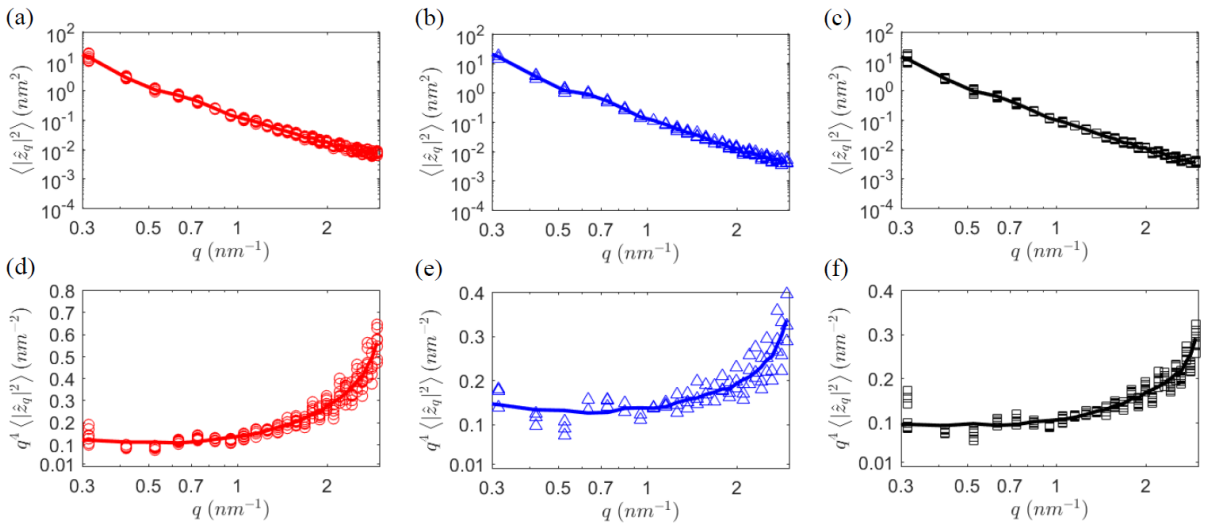

FIG. 10. Time averaged undulation spectra for a) DOPC, b) DOPE and c) DOPG bilayer, normalized undulation spectra for d) DOPC, e) DOPE and f) DOPG bilayer with δ=2nm, α=8 and N=32.

obtained from experimental investigation and from equivalent computational techniques published earlier. The different lipid types studied here (DOPC, DOPE, DOPG) result in similar estimates for the bending moduli i.e. 12-13$\times 10^{-20}$J highlighting that the differences in the head groups for these lipid types do not significantly affect the bending moduli. However, the bending moduli for these lipids is significantly smaller ($\sim$25%) than those estimated for a DPPC bilayer presented in Section V.1 from experimental investigation and orientation analysis. Thus, the difference in the tail group for the lipids is observed to lead to a larger change in bending modulus estimates.

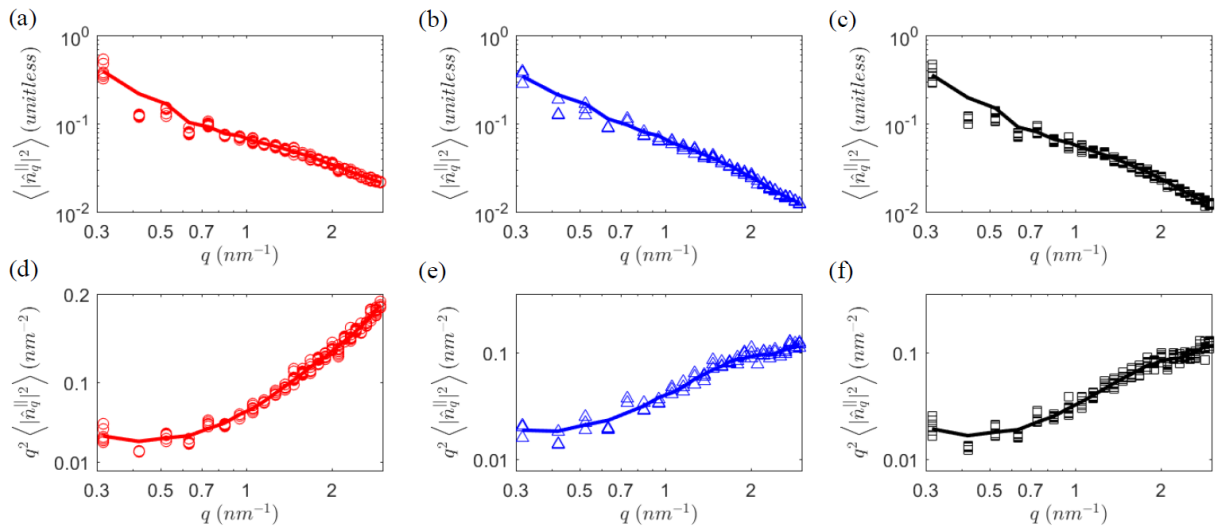

FIG. 11. Time averaged orientation spectra for a) DOPC, b) DOPE and c) DOPG bilayer, normalized orientation spectra for d) DOPC, e) DOPE and f) DOPG bilayer with δ=2nm, α=8 and N=32.

VI. CONCLUSION

In the current work, estimates of bending modulus for homogeneous lipid bilayer membranes are studied using the undulation and orientation analysis of coarse-grained molecular trajectories. A weighted horizon based averaging scheme is proposed to interpolate the molecular trajectories from unstructured data to a structured grid. The weighted horizon based averaging scheme presented reduces issues with empty cells and provides a finer grid for Fourier analysis improving the resolution and accuracy of the bending modulus estimates. The effect of key interpolation parameters in weighted averaging of molecular trajectories and subsequent Fourier analysis are systematically investigated using parametric studies. It is observed that the choice of these interpolation parameters may influence the estimated moduli and the key consideration is retaining the local perturbations in the trajectories as far as possible to obtain converged results.

The computational analysis is verified with computational and experimental characterization of bilayer bending moduli published in the literature and validated with experimental characterization performed herein. It is observed that the orientation analysis predicts bending moduli which are closer to experimentally observed results as compared to the undulation analysis, as noted in an earlier study [9]. The computational framework is further used to

TABLE V. Bilayer bending modulus reported for different lipid types from computational and experimental studies in the literature in comparison to those estimated in the current work.

Reference	Type of Study	Size (number of lipids), time (μs)	k_c ($\times 10^{-20}$J)
Previously Published Literature			
DOPC [16]	Orientation Analysis (CHARMM)	648, 0.17	11.4
DOPC [9]	Buckling Analysis (MARTINI)	640, 4	15.5
DOPE [16]	Orientation Analysis (CHARMM)	648, 0.14	11.4
DOPC [21]	Shape Fluctuation Analysis (Experimental)	-	11.0
DOPC [36]	Shape Fluctuation Analysis (Experimental)	-	9.0-12.0
Current Work			
DOPC	Undulation Analysis (MARTINI)	3200, 0.4	3.84
DOPC	Orientation Analysis (MARTINI)	3200, 0.4	12.08
DOPE	Undulation Analysis (MARTINI)	3200, 0.4	3.17
DOPE	Orientation Analysis (MARTINI)	3200, 0.4	12.01
DOPG	Undulation Analysis (MARTINI)	3200, 0.4	4.72
DOPG	Orientation Analysis (MARTINI)	3200, 0.4	12.98

study lipids of the same size, but, with different head and tail groups. It is observed that the bending moduli are more sensitive to differences in tail groups as compared to the head groups. The current work sheds further light on the numerical analysis techniques for estimating bilayer bending moduli and establishes the difference in these estimates for different lipid types.

VII. ACKNOWLEDGEMENT

The authors would like to acknowledge support from National Science Foundation - Molecular and Cellular Biosciences (Grant No. 1244014). The authors also acknowledge the facilities and support staff at Georgia Advanced Computing Resource Center (GACRC).

[1] S. Kawamoto and W. Shinoda, Soft Matter **10**, 3048 (2014).

[2] P. M. Kasson and V. S. Pande, PLoS Computational Biology **3**, 2228 (2007).

[3] S. Kawamoto, M. L. Klein, and W. Shinoda, The Journal of Chemical Physics **143**, 243112 (2015).

[4] E. Lindahl and O. Edholm, Biophysical Journal **79**, 426 (2000).

[5] E. G. Brandt, A. R. Braun, J. N. Sachs, J. F. Nagle, and O. Edholm, Biophysical Journal **100**, 2104 (2011).

[6] E. R. May, A. Narang, and D. I. Kopelevich, Physical Review E **76**, 021913 (2007).

[7] W. Helfrich, Zeitschrift fr Naturforschung C **28**, 693 (1973).

[8] P. B. Canham, Journal of Theoretical Biology **26**, 61 (1970).

[9] D. Bochicchio and L. Monticelli, "Chapter five - the membrane bending modulus in experiments and simulations: A puzzling picture," in *Advances in Biomembranes and Lipid Self-Assembly*, Vol. Volume 23 (Academic Press, 2016) pp. 117–143.

[10] J. F. Nagle, M. S. Jablin, S. Tristram-Nagle, and K. Akabori, Chemistry and Physics of Lipids **185**, 3 (2015).

[11] M. C. Watson, E. G. Brandt, P. M. Welch, and F. L. Brown, Physical Review Letters **109**, 028102 (2012).

[12] M. C. Watson, E. S. Penev, P. M. Welch, and F. L. Brown, The Journal of Chemical Physics **135**, 244701 (2011).

[13] O. Edholm, Current Topics in Membranes **60**, 91 (2008).

[14] B. Rozycki and R. Lipowsky, The Journal of Chemical Physics **142**, 1 (2015).

[15] M. Hu, P. Diggins IV, and M. Deserno, The Journal of Chemical Physics **138**, 214110 (2013).

[16] Z. A. Levine, R. M. Venable, M. C. Watson, M. G. Lerner, J.-E. Shea, R. W. Pastor, and F. L. Brown, Journal of the American Chemical Society **136**, 13582 (2014).

[17] M. C. Watson, A. Morriss-Andrews, P. M. Welch, and F. L. Brown, The Journal of Chemical Physics **139**, 1 (2013).

[18] S. J. Marrink, A. H. De Vries, and A. E. Mark, The Journal of Physical Chemistry B **108**, 750 (2004).

[19] S. J. Marrink, H. J. Risselada, S. Yefimov, D. P. Tieleman, and A. H. De Vries, The Journal of Physical Chemistry B **111**, 7812 (2007).

[20] S. J. Marrink and D. P. Tieleman, Chemical Society Reviews **42**, 6801 (2013).

[21] Y. Elani, S. Purushothaman, P. J. Booth, J. M. Seddon, N. J. Brooks, R. V. Law, and O. Ces, Chemical Communications **51**, 6976 (2015).

[22] P. Meleard, C. Gerbeaud, P. Bardusco, N. Jeandaine, M. Mitov, and L. Fernandez-Puente, Biochimie **80**, 401 (1998).

[23] J. R. Henriksen and J. H. Ipsen, The European Physical Journal E: Soft Matter and Biological Physics **14**, 149 (2004).

[24] Y. Lyatskaya, Y. Liu, S. Tristram-Nagle, J. Katsaras, and J. F. Nagle, Physical Review E **63**, 011907 (2000).

[25] R. Dimova, Advances in Colloid and Interface Science **208**, 225 (2014).

[26] H. Bouvrais, Advances in Planar Lipid Bilayers and Liposomes, Vol 15 **15**, 1 (2012).

[27] P. Meleard and T. Pott, Advances in Planar Lipid Bilayers and Liposomes **17**, 55 (2013).

[28] V. Vitkova and A. G. Petrov, Advances in Planar Lipid Bilayers and Liposomes **17**, 89 (2013).

[29] T. A. Wassenaar, H. I. Ingolfsson, R. A. Bockmann, D. P. Tieleman, and S. J. Marrink, Journal of Chemical Theory and Computation **11**, 2144 (2015).

[30] I. R. Cooke and M. Deserno, The Journal of Chemical Physics **123**, 224710 (2005).

[31] T. J. Politano, V. E. Froude, B. Jing, and Y. Zhu, Colloids and Surfaces B: Biointerfaces **79**, 75 (2010).

[32] P. Meleard, L. A. Bagatolli, and T. Pott, Methods in Enzymology **465**, 161 (2009).

[33] Y. Okumura and Y. Iwata, Membranes **1**, 109 (2011).

[34] M. M. Lapinski, A. Castro-Forero, A. J. Greiner, R. Y. Ofoli, and G. J. Blanchard, Langmuir **23**, 11677 (2007).

[35] Y. Z. Yoon, J. P. Hale, P. G. Petrov, and P. Cicuta, Journal of Physics: Condensed Matter **22**, 062101 (2010).

[36] L. Fernandez-Puente, I. Bivas, M. Mitov, and P. Meleard, EPL (Europhysics Letters) **28**, 181 (1994).